





## Article

# Biocompatibility Assessment of Coatings Obtained in Argon and Nitrogen Atmospheres for TiNi Materials

Ekaterina Marchenko , Gulsharat Baigonakova \* , Oleg Kokorev , Yuri Yasenchuk   
and Alexander Vorozhtsov

Laboratory of Superelastic Biointerfaces, National Research Tomsk State University, 36 Lenin Ave.,  
634045 Tomsk, Russia

\* Correspondence: gat27@mail.ru

**Abstract:** This work aims to study the cytocompatibility of protective coatings obtained in argon and nitrogen atmospheres on a TiNi surface. Particular attention is paid to comparing the interaction of cell culture with coatings and an uncoated TiNi sample, using for comparison the number of viable cells on the surface, the phase composition, structure, wettability, surface charge and topography. The Ti/Ni/Ti nanolaminate was deposited on a TiNi substrate by magnetron sputtering. Reaction annealing of Ti/Ni/Ti nanolaminate on a TiNi substrate, when heated to 900 °C in argon, leads to the formation of a dense two-layer coating 2.0–2.1 µm thick: layer I (TiO + Ti<sub>2</sub>N), layer II (Ti<sub>4</sub>Ni<sub>2</sub>O(N)). Reaction annealing in nitrogen leads to the formation of a thin three-layer nanocoating 250 nm thick: I (TiO<sub>2</sub> + TiN), II (Ti<sub>4</sub>Ni<sub>2</sub>N(O) + Ti<sub>3</sub>Ni<sub>4</sub>), III (TiN). The coating synthesized in nitrogen is more favorable for cell attachment and proliferation because of the moderately hydrophilic rough surface and mixed phase composition of titanium nitrides and oxides.



**Citation:** Marchenko, E.; Baigonakova, G.; Kokorev, O.; Yasenchuk, Y.; Vorozhtsov, A. Biocompatibility Assessment of Coatings Obtained in Argon and Nitrogen Atmospheres for TiNi Materials. *Metals* **2022**, *12*, 1603. <https://doi.org/10.3390/met12101603>

Academic Editor: Yadir Torres Hernández

Received: 31 August 2022

Accepted: 21 September 2022

Published: 26 September 2022

**Publisher's Note:** MDPI stays neutral with regard to jurisdictional claims in published maps and institutional affiliations.



**Copyright:** © 2022 by the authors. Licensee MDPI, Basel, Switzerland. This article is an open access article distributed under the terms and conditions of the Creative Commons Attribution (CC BY) license (<https://creativecommons.org/licenses/by/4.0/>).

**Keywords:** coating; cell adhesion; magnetron sputtering; reaction annealing; nickel titanium

## 1. Introduction

The corrosion resistance of protective coatings has great importance for the cytocompatibility of metal implants. The protective coating protects the metal implant base from dissolution by tissue fluids and prevents the harmful effect of toxic metal ions on the cells that form the biointerface. With prolonged exposure to physiological load and stress in a corrosive biological environment, metal implants release toxic metal ions, which penetrate the surrounding tissues of the body [1–3]. Titanium nitride coatings, which are wear resistant, durable and FDA approved, are the most effective in preventing these processes [4–8].

The application of thin films of titanium nitride has become a promising way of modifying the surface of metal implants due to chemical stability and corrosion resistance. The hydrophilic nature of nitride coatings allows for protein adsorption. In vitro biocompatibility studies have demonstrated that the coatings are non-toxic and exhibit excellent interactions between cells and materials. The surface morphology of titanium nitride coatings depends on the method and modes of deposition. Within one coating method, the morphology of its surface varies from smooth to island to sharply crystalline, depending on temperature, pressure, nitrogen flow rate and nitrogen ratio in the gas mixture [9–12]. In all cases, nitrogen atoms diffuse through the surface layer of titanium, moving through octahedral interstices of the titanium lattice [13,14]. Nitride coatings have different application times. Coatings sputtered for 80 min have better tribocorrosion properties compared to coatings sputtered within 30 min [15]. As the deposition time increases, a thicker and less permeable film is formed.

The deposition temperature affects the phase composition of titanium nitride films. Diffusion and dissolution of nitrogen in the titanium lattice at a temperature of 400 °C

lead to the formation of an  $\alpha$ -solid solution of nitrogen in titanium. At a temperature of 500 °C, the nitrogen concentration in titanium increases and the  $Ti_2N$  phase is formed, and starting from a temperature of 550 °C, a two-phase state of  $TiN + Ti_2N$  is observed. A further increase in temperature leads to a complete rearrangement of the crystal lattice into a cubic one and the formation of the  $TiN$  phase [16]. A similar sequence of phase formation is retained in a gas mixture of nitrogen with argon with an increase in the nitrogen concentration [10]. During cathodic arc deposition on titanium alloy, the  $TiN$  coating has shown a high hardness of  $33.4 \pm 10$  GPa and Young's modulus of  $458.4 \pm 79$  GPa. Investigation of the interface microstructure between the coating and the substrate revealed the high quality and uniformity of the coating along the surface. In addition,  $TiN$  has been shown to exhibit excellent biocompatibility, wear resistance and wettability, and the bioactivity of these coatings is also excellent due to the adsorption of proteins present in body fluids [17,18]. Evaluation of the wettability and corrosion resistance, mechanical and tribological properties of the  $TiN$  coating demonstrated its promising application as an implant material on Ti and  $TiNi$  alloys. Comparison of the viability of NIH3 T3 cells on a  $Ti6 Al4 V$  alloy substrate without a coating and with a  $TiN$  coating showed a high cytocompatibility of the coating [18]. Cells multiplied faster on  $TiN$  coatings, and showed clear extensions of filopodia and intercellular contacts, demonstrating that all samples provided early cell adhesion. With an increase in the cultivation duration on  $TiN$  coatings, the number of cells rapidly increases and they completely cover the sample [17].  $TiN$  deposited using a high-power pulsed magnetron sputtering technique exhibits high polarization resistance in simulated body fluid and demonstrates excellent MG63 osteoblast-like cell viability [19]. Analysis of the cytocompatibility of thin  $TiBN$  films showed increased compatibility with cells and toxicity of these coatings [20–22]. The  $TiN$  coating can enhance cell attachment, proliferation and proliferation on  $NiTi$ . The results showed that the  $TiN$  coating adheres well to the substrate, withstanding a load of 4099 N after bending to a displacement of 2 mm, and can lead to better biocompatibility due to greater roughness and good wettability [4].

Titanium oxide coatings exhibit a wide range of structural and chemical properties. There are different methods of obtaining coatings, for example, when exposed to an atmosphere of air and flowing argon, thermal and electrochemical oxidation, magnetron sputtering, etc. [21–25]. Titanium oxide coatings are known for their high biocompatibility by increasing cytocompatibility, reducing metal corrosion and toxic ion release. Titanium oxide coatings due to their microporous and large surface area facilitate the attachment of osteoblasts to the implant surface [16]. This is due to a significant increase in the area and wettability of the microporous surface of the sample. Surface modification in vitro at different periods of osteoblast cell cultivation was studied in [1]. In [26], the nanostructured oxide layer improved the bioactivity, hemocompatibility and osseointegration of titanium plate.

Interest in titanium oxynitride coatings is due to high biocompatibility, cytocompatibility, corrosion resistance and wear resistance [27,28]. Titanium oxynitrides with different oxygen content ( $TiNO_x$ ) have properties that are superior to titanium nitrides and titanium oxides [29]. There are positive results from a clinical study of  $TiNO_x$ -based coatings for stainless steel stents. The compatibility of the titanium oxide coating with blood in terms of platelet adhesion and fibrinogen adsorption can be improved by adding nitrogen to it. When studying the interaction of various types of  $TiO_x$  and  $TiO_xNy$  coatings with EA.hy926 endothelial cells, none of the tested samples showed cytotoxicity, while increasing the biocompatibility of  $NiTi$  stents [30]. In [8], the authors created a mechanically protective and biofunctional surface by combining  $TiN$  with bioactive nanostructured  $TiO_2$  deposited on it. The results showed that the  $TiN/TiO_2$  is more favorable for cell attachment and proliferation of MG63 osteoblasts, providing a better environment for cell growth compared to pure alloys [31].

It is known that argon is an inert gas, and nitrogen is a reaction gas, which chemically interacts with titanium and forms titanium oxynitride phases. In inert argon, there are

always residual impurities of nitrogen, oxygen and carbon, which react with titanium. As a consequence, the surface morphology of the films upon annealing in air, argon, nitrogen, or carbon can be similar but undergoes changes depending on the crystallization kinetics [9–14,32–34].

Implantable materials for long-term functioning in the body must contain their vasculature, therefore, they must be tested for hemocompatibility. When biotesting materials, in contact with the circulatory system, the greatest attention is paid to the effect of the sample on blood cells, i.e., primarily on the reaction of erythrocytes. Sedimentation and cell adhesion are the initial processes of cell interaction with the implant surface, which significantly affect the integration of the implant and the success of the functioning of the implant–biological tissue interface [35]. The compatibility of thin films with blood is studied by monitoring the morphology and aggregation of platelets with platelet-rich plasma since adhesion of blood cells is one of the main problems during thrombus formation on the surface of a biomaterial. Evaluation of cytocompatibility is carried out using tests for hemolysis, MTT tests and screening control of matrix properties of cells using confocal microscopy.

Surface characteristics of biomedical implants, including morphology, surface topography, chemical distribution, phase composition, charge state, surface free energy and wetting properties, affect their interaction with cells and the extracellular matrix, namely the adaptation, mobility and viability of cells on the surface [36]. To assess the localization and viability of cells on the surface of a biomaterial, it is necessary to carry out a comparative study of the surface characteristics, that emphasizes the relevance of this study.

This work aims to study the effect of the phase composition, structure, wettability, surface charge and topography of protective coatings obtained in argon and nitrogen atmospheres on the distribution of cells on the TiNi surface. Particular attention is paid to comparing the distribution of cells over coatings obtained in argon and nitrogen and on the surface of an uncoated TiNi sample, using for comparison the number of viable cells on the surface and the regularities of filling and spreading of the surface with cells.

Additionally, the novelty of the work consists in the fact that a comparative analysis of the formation of a coating under different gaseous atmospheres on TiNi alloys has not been carried out and the surface properties have not been studied from the point of view of interaction with a cell culture. In the previous works of the authors, the stage-by-stage creation of coatings and the effect of gaseous impurities on the phase composition and structure of coatings at different synthesis temperatures were considered.

## 2. Materials and Methods

### 2.1. Deposition of the Amorphous Ti/Ni/Ti Nanolaminate and Synthesis of Coating

For comparative analysis, coatings were obtained by reaction annealing at a temperature of 900 °C in two different atmospheres: in argon and nitrogen. Plates of polycrystalline titanium nickelide with dimensions of 10 × 10 × 2 mm were used as a substrate. Amorphous Ti/Ni/Ti layers with thicknesses of 50/50/50 nm were magnetron sputtered alternately in high-purity argon using Ti and Ni targets 80 mm in diameter with a 1 kV, 5 A DC source on TiNi substrates. Experimentally chosen deposition modes were as follows: Ar working pressure of 1 Pa; deposition time of 75 s (Ti) and 30 s (Ni); discharge voltage of 350 V (Ti) and 420 V (Ni), magnetron current of 1 A (Ni) and 2 A (Ti), substrate temperature equal to room temperature, argon flow  $\phi_{Ar}$  of 35 sccm, floating potential ( $\approx 25$  V) for the substrate displacement. The distance from the substrate to the targets was 100 mm. In these conditions, the operating deposition rates were determined to be 40 nm/min for titanium and 100 nm/min for nickel. After deposition of the Ti/Ni/Ti nanolaminate, the samples were heated to 900 °C in an argon atmosphere and a nitrogen atmosphere using a heated graphite substrate holder and held at this temperature for 60 s (Figure 1). In the case of annealing nanolaminate in a nitrogen atmosphere, argon was evacuated from the chamber to a base pressure of  $8 \times 10^{-4}$  Pa, and nitrogen gas was pumped at an operating pressure of

1 Pa without removing samples. After heating, the samples were cooled together with the chamber in a nitrogen atmosphere at 1 Pa to room temperature for 60 min.

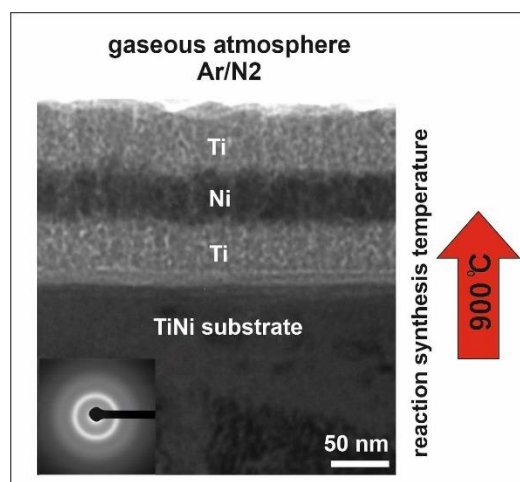


**Figure 1.** Scheme of deposition of the amorphous Ti/Ni/Ti nanolaminate and synthesis of coating.

## 2.2. Cytocompatibility and Hemolysis Test

To study cytocompatibility, the samples were degreased with 70% ethanol, washed in an ultrasonic bath, autoclaved at 180 °C for an hour. Next, the samples were washed three times with culture medium and placed in a 24-well plate.

### 2.2.1. Hemolysis Test

The blood of a healthy volunteer was used with a solution, containing sodium citrate (3.8 wt.%). In a ratio of 9:1, it was diluted with saline (ratio 4:5 by volume). The samples were immersed into a standard tube containing 10 mL of physiological saline that had been preincubated at 37 °C for 30 min. Next, 0.2 mL of diluted blood was added to this standard tube and the resulting mixture was incubated for 60 min at 37 °C. Similarly, 0.85% NaCl physiological saline was used as a negative control and deionized water was used as a positive control. Thereafter, all tubes were centrifuged for 5 min at 3000 rpm, and the supernatant was transferred to a cuvette for spectroscopic analysis at a wavelength of 545 nm. Hemolysis was calculated using an ultraviolet spectrophotometer (Pikon Inc., Uniplan, RF) at 545 nm. Hemolysis percent is the average of three replicates and was calculated as (Equation (1)):

$$\text{Hemolysis} = \frac{(\text{OD (test sample)} - \text{OD (negative control)})}{((\text{OD (positive control)} - \text{OD (negative control)}))} \times 100\%, \quad (1)$$

where OD—test sample extinction index, OD (negative control)—negative control extinction index, OD (positive control) is a measure of the extinction of the positive control.

### 2.2.2. MTT Test

To assess the cytotoxicity of uncoated TiNi substrate and coatings, MCF-7 cells were cultured in Dulbecco's modified Eagle medium (DMEM) (Paneco, RF) with 10% fetal bovine serum (FBS), antibiotics (100 U/mL of penicillin and 100 mg/mL of streptomycin) and 2 mM L-glutamine at 37 °C in 5% CO<sub>2</sub>. The cytotoxicity tests were performed by direct contact. The control groups involved the use of DMEM as a negative control and 0.64% phenol DMEM as a positive control. Cells were incubated in 12-well plates for 24–72 h. Thereafter, MTT was added to each well. The samples were incubated with MTT for 4 h at 37 °C, the plates were centrifuged for 10 min at 1500 rpm, the supernatant was carefully removed, and solution of solubilized formazan (10% SDS in 0.01 M HCl) was added to each well. The spectrophotometric absorbance of the samples was measured at 540 nm on a Uniplan spectrophotometer (Pikon Inc., RF) with a reference wavelength of

630 nm. Percent of cytotoxicity is the average of three replicates and was calculated as (Equation (2)):

$$\text{Cytotoxicity} = \frac{O - K}{O} \times 100\%, \quad (2)$$

where O is the extinction index of the test sample, K is the extinction index of the control sample.

For screening testing of matrix properties, an epithelial tumor cell line of the human breast duct, MCF-7, was used. It is one of the most commonly used cell lines with the characteristics of differentiated epithelium for in vitro studies of the cytotoxicity of anticancer pharmaceuticals, molecular biology of cancer, as well as cytocompatibility of various biocompatible materials. The main functional ability of these cells is adhesion to the substrate, spreading and population growth. It is easy to compare the viability of cells on surfaces with different physicochemical properties for the listed group of characteristics.

Fluorescence of the samples from 10 mm × 10 mm surface areas with cells was visualized using the LSM-780 NLO Confocal Laser Scanning Microscope, (Carl Zeiss Microscopy GmbH, Jena, Germany). Cells were visualized using double staining with acridine orange and ethidium bromide. For staining, the samples were prewashed from the medium and flooded with the working dye solution for 10 min. Live cells (green cells) were stained with acridine orange, and dead cells (red cells) were stained with ethidium bromide. Fluorescent acridine orange was excited using a laser with a wavelength of 488 nm, and fluorescence was recorded in the range of 495–545 nm. Fluorescent ethidium bromide was excited using a laser with a wavelength of 561 nm, and fluorescence was recorded in the range of 580–690 nm. As a result, fluorescent images of localizations of acridine orange (green) and ethidium bromide (red), and an image obtained in the transmitted light mode, were superimposed.

### 2.3. Surface Characterization Methods

The surface structure of the outer layer was investigated using a TESCAN VEGA3 scanning electron microscope (Tescan, Brno, Czech Republic). The topography and surface charge of the coating were investigated by atomic force microscopy (AFM, NT-MDT LLC, Moscow, RF). AFM employed an NT-MDT scanning probe microscope with a SOLVER HV vacuum chamber in a semi-contact mode. Data processing was performed using the Gwyddion program.

The contact wetting angle was determined by the sessile droplet method at room temperature using an EasyDrop DSA20 E device (KRÜSS, Hamburg, Germany). The sessile droplet volume was 5 µL. The measurement accuracy was ±1 angular degree. The test liquids were water with known free energy of the surface and its components. The contact angle values were used to calculate the surface wettability and free energy. The free surface energy was calculated by the Ouns, Wendt, Rabel and Kjellble method as the sum of polarization and dispersion components.

## 3. Results and Discussion

### 3.1. Hemolysis and MTT Test

As part of the screening control for cytocompatibility, an assessment of membranotoxic and cytotoxic activity, morphology and density of cells on the surface of a biomaterial was carried out, showing an increase or decrease in the cell population in a time interval. When implanting metal materials into the body, the reaction of cells is determined by the surface state. The morphology of cells provides qualitative information about the cell–surface interaction. For example, premature extension of filopodia, a reduced amount of filopodia and round shape imply poor cell–surface interaction [18]. With a biochemically incompatible surface, a fibrous capsule appears around the implant, which prevents cell adhesion and proliferation, leading to failure and further rejection of the implant.

The erythrocyte hemolysis test shows the interaction of the entire surface of the biomaterial with blood cells, which are necessary for the oxygen transfer by the blood to



tissue cells and promoting their oxidative processes. Samples with coatings showed values of erythrocyte hemolysis of  $1.2\% \pm 0.2$  and  $0.9\% \pm 0.15$ , which do not exceed the allowed values of about 2% according to ISO 10993–4:2018 for hemolysis by biomaterials in contact with blood. At the same time, the uncoated TiNi substrate causes a degree of hemolysis of  $3.6\% \pm 0.8$ , which is higher than the tolerable standard ISO 10993–4:2018. This indicates that this sample is undesirable (Figure 2).

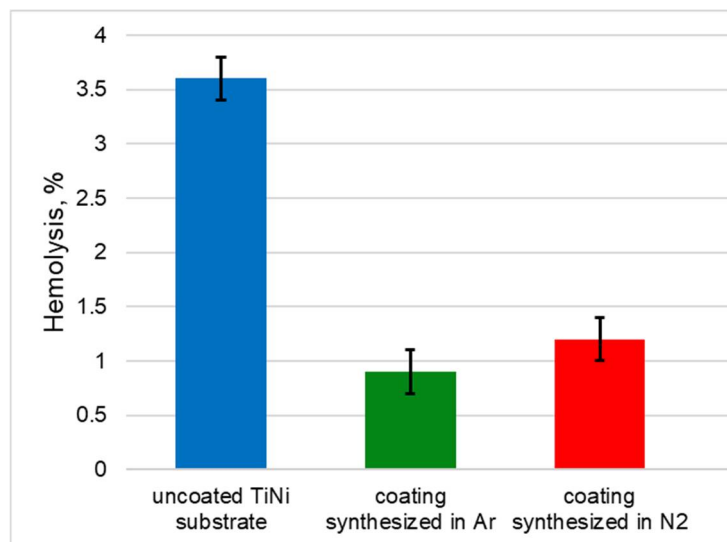


**Figure 2.** Percentages of erythrocyte hemolysis.

In the cytotoxicity study of the samples, the MTT test with MCF-7 cells after 24 h showed that the uncoated TiNi substrate has the highest cytotoxicity of  $34\% \pm 4.1$ . The next in order of decreasing percentage of cytotoxicity is the coating synthesized in an argon atmosphere with a cytotoxicity index of  $23\% \pm 3.1$ . A coating synthesized in a nitrogen atmosphere has the lowest cytotoxicity index of  $12\% \pm 2.3$ , which is 22% less than the cytotoxic index of the substrate (Figure 3).

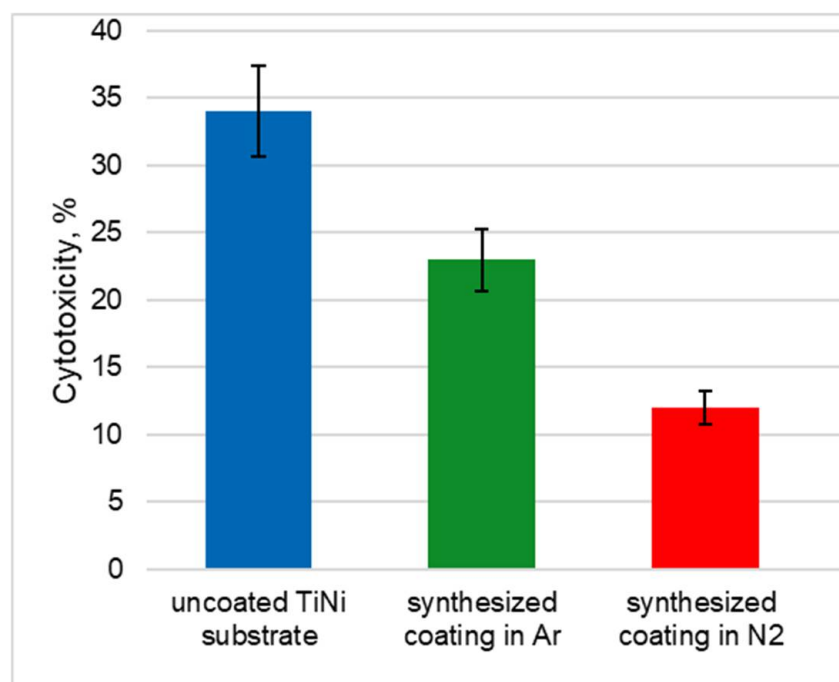


**Figure 3.** Cytotoxicity towards MCF-7 cells after 24 h.

The results of microscopic investigation of MCF-7 cell adhesion after 72 h on the surface of the samples correlate with the cytotoxicity index (Figure 3). On the uncoated TiNi sample after 72 h of cultivation, MCF-7 cells were found attached to the surface (Figure 4a). The population is represented mainly by flattened functional cells, which occupied less than 50% of the area seeded by cell populations. At the same time, they retained the typical morphology characteristic of this cell line, but their size is significantly smaller than in other studied samples. Evaluating the small number of cells attached to the surface, it can be concluded that the surface of this sample is less cytocompatible for the cells of this line compared to other studied samples.

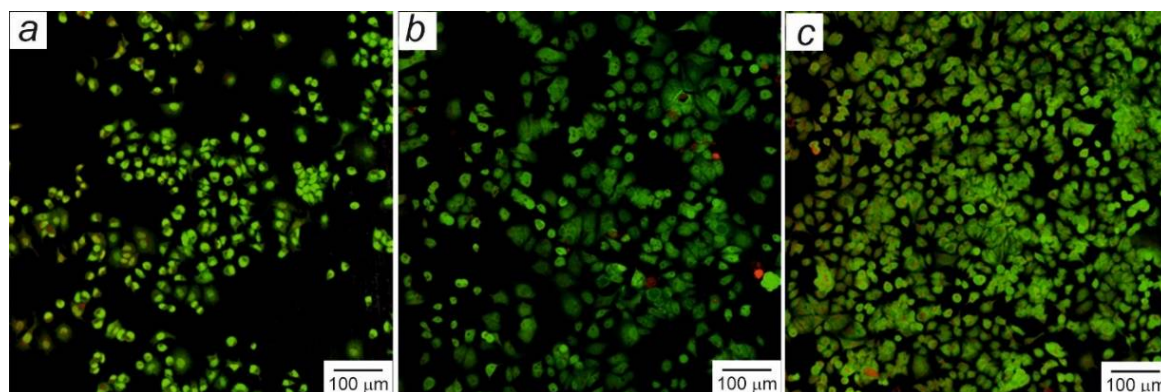


**Figure 4.** Confocal laser microscopy of samples after 72 h culture with MCF-7 cells: uncoated TiNi substrate (a), coating synthesized in an argon atmosphere (b), coating synthesized in a nitrogen atmosphere (c).

After 72 h of cultivation, the cells covered more than 70% of a sample surface area of  $1 \times 1 \text{ mm}^2$  with a coating synthesized in argon (Figure 4b). Group accumulations of viable spread cells and 2–3 dead cells in the field of view were found. Staining with all red nuclear dye indicates the release of nuclear material during cell death. The number of viable cells attached to the surface of this sample and their size is much larger than on the TiNi substrate, but visually their number is less than on the coating synthesized in nitrogen. The coating synthesized in nitrogen showed the highest number of MCF-7 cells (Figure 4c). This indicates the best primary adhesion of intact cells and an increase in the population of these cells within 72 h. Most of the cells changed from their primary rounded shape to an elongated flattened one, which indicates better surface compatibility with this type of cell compared to an uncoated sample. The cell mass on the surface practically covers the entire surface of the sample with a monolayer with characteristic dense cell foci with increased adhesive activity. This fact indicates a better cytocompatibility of the coating synthesized in nitrogen.

It was found that the density of filling the surfaces with cells correlates with their cytotoxicity index. The most cytotoxic intact substrate sample has the lowest cell filling density, where cell clusters are represented by separate local areas. Samples with synthesized coatings are less cytotoxic and have a higher density of cell surface coverage. The adhesion of a larger number of cells to their surfaces allows them to maintain their viability for a longer period than an intact sample. At the same time, on the sample with the coating synthesized in nitrogen, the contours of the cell colonies were not detected, as in the case of other samples, since the spread cells are dense and cover most of the surface.

At the beginning of the experiment, the number of cells deposited on the surface of all samples was approximately equal. At the end of the experiment, the filling density changed. During the preparation of the sample for microscopy, dead non-adherent cells were washed away. Some of the dead cells, colored red, remained adherent to the surface. On the surface of the TiNi substrate and the coating synthesized in argon, there are agglomerates of adhered cells 50–70 µm in size, and on the surface of the coating synthesized in nitrogen, the agglomerates reach 150 µm. As a result of washing away the dead cells, rounded

cell-free areas were formed: the dimensions of the areas in the sample of the substrate are 70–300  $\mu\text{m}$ , on the coating synthesized in argon—20–50  $\mu\text{m}$ , on the coating synthesized in nitrogen—25–150  $\mu\text{m}$ . Cell-free areas indicate some local areas that are not favorable for cell life. Thus, on the surface of uncoated TiNi substrate, these areas are more common and their influence is stronger than on samples with coatings.

### 3.2. Structural Studies of Coatings Synthesized in Argon and Nitrogen Atmospheres

#### 3.2.1. Structural Studies

The outer layer of the coating synthesized in argon is porous with an island morphology, formed by agglomerates of intergrown grains with a size of 1–2  $\mu\text{m}$ . The pores between the agglomerates are 1–3  $\mu\text{m}$  in size (Figure 5a). The outer layer of the coating synthesized in a nitrogen atmosphere has an even more pronounced island morphology, formed by agglomerates of intergrown grains less than 1  $\mu\text{m}$  in size. The pores between the agglomerates are 1–2  $\mu\text{m}$  in size (Figure 5b). The outer layer of coatings obtained both in argon and nitrogen is permeable and cannot perform a protective function. However, the microgranular islet-type relief is favorable for the deposition, adhesion and proliferation of cells.

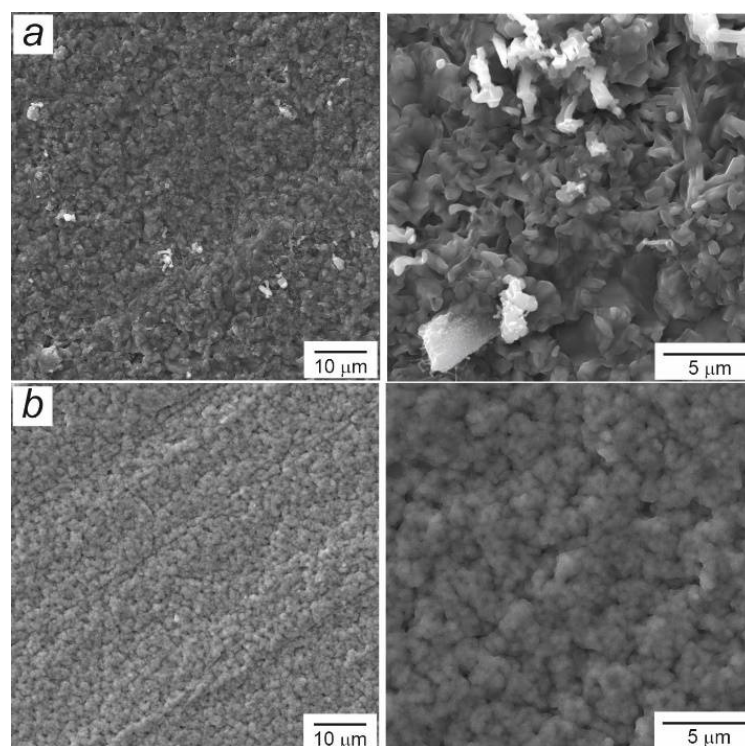


**Figure 5.** SEM images of surface morphology: coating synthesized in an argon atmosphere (a), coating synthesized in a nitrogen atmosphere (b).

In our previous works, XRD results showed that the outer layer of the coating synthesized in a nitrogen consists of  $\text{TiO}_2$  and  $\text{TiN}$ , and when synthesized in argon of  $\text{TiO}$  and  $\text{Ti}_2\text{N}$ , which indicates less completeness of the conversion of the synthesis reaction in argon [32,34]. It is known that titanium nitride compounds are more prone to the formation of dense columnar crystalline coatings, and titanium oxides are more prone to the formation of loose gradient island coatings.

Furthermore, TEM analysis showed that the reaction synthesis of Ti/Ni/Ti nanolaminate on a TiNi substrate in argon at a temperature of 900  $^\circ\text{C}$  leads to the formation of a dense two-layer coating of 2.0–2.1  $\mu\text{m}$  thick [32]. The coating is connected to the substrate by a diffusion zone of 2.5–2.7 microns. During the reaction annealing, solid-phase diffusion–reaction processes are initiated between the Ti/Ni/Ti nanolaminate layers and



the TiNi substrate. Diffusion growth was induced under the influence of directed diffusion of titanium and oxygen into the nickel layer, as evidenced by the columnar structure of continuous crystalline layers of the coating. The structural features of the formation of a two-layer coating in the form of a structure of columnar grains are in good agreement with a third zone of the Movchan–Demchishin model [37], in which, at temperatures above  $0.45 T_{\text{melt}}$  (at  $900\text{ }^{\circ}\text{C}$  for titanium and nickel it is 0.54 and 0.62, respectively), the coating takes the form of equiaxed grains due to bulk diffusion. Structure results showed that layer I contains a greater amount of oxygen, due to which the concentration boundary between layers I and II is visible. It follows from the concentration ratios of the Ti, O, N elements that layer I consists of the  $\text{TiO} + \text{Ti}_2\text{N}$  phases and layer II of  $\text{Ti}_4\text{Ni}_2\text{O}(\text{N})$ . Nickel was not found in the outer coating layer. It is assumed that the outer layer prevented the diffusion of nickel to the surface, but it diffused towards the substrate together with interstitial impurities. As a result, the Ni layer dissolved in the titanium layer and reacted with it up to the  $\text{Ti}_2\text{Ni}$  stoichiometry. A layer of  $\text{Ti}_4\text{Ni}_2\text{O}(\text{N})$  oxynitride crystallized during interaction with interstitial impurities. In this case, the near-surface layers of the TiNi(B2) substrate modified into a diffusion zone with inclusions of the  $\text{TiNi}_3$  phase.

In previous work [34], the authors showed that the reaction synthesis of Ti/Ni/Ti nanolaminate on a TiNi substrate by heating to  $900\text{ }^{\circ}\text{C}$  in a nitrogen atmosphere leads to the formation of a coating of 250 nm thick with a gradient crystal structure. As a result of reaction annealing, a dense coating of three crystalline layers I, II, III was formed. Layer I has an average thickness of about 150 nm with an average size of grains of about  $40 \pm 5\text{ nm}$ . The denser layers II and III have approximately equal thicknesses of about 50 nm and nanosized grains of about  $8 \pm 2\text{ nm}$ . A diffusion zone with a thickness of about 230 nm was formed in the substrate and bonded the substrate to the coating.

The EDS maps show that the outer layer I consists of the elements Ti, N, O and does not contain Ni. A noticeable concentration of Ni was found in the diffusion zone  $\text{DZ}_B$  and layer II, and insignificant depletion in titanium was found in these layers. Oxygen is relatively uniformly distributed up to the diffusion zone  $\text{DZ}_A$ , beyond which its concentration decreases. This distribution of elements suggests that oxygen is adsorbed from argon. Such content of oxygen atoms can be associated with the participation of residual oxygen in the nanolaminate during the deposition in an argon atmosphere and annealing in a nitrogen atmosphere, as well as with oxygen diffusion from the TiNi substrate. The formed layer I should preferably consist of a larger amount of TiN since the nitrogen content prevails in the atmosphere, which is further shown by XRD results. In intermediate layer II, oxynitride  $\text{Ti}_4\text{Ni}_2\text{N}(\text{O})$  and  $\text{Ti}_3\text{Ni}_4$  phases were formed. The titanium nitride layer III inhibits the further diffusion of nitrogen into the DZ zone. The concentration of the elements Ti, Ni, O indicates that the  $\text{DZ}_A$  layer is a  $\text{TiNiO}_3$  phase. According to the EDS results, the atomic percentage of Ni and Ti in the  $\text{DZ}_B$  zone is 3:1, which corresponds to the  $\text{TiNi}_3$  phase.

The X-ray diffraction analysis is consistent with the EDS results for coatings obtained in argon and nitrogen. X-ray diffraction patterns show that after synthesis at  $900\text{ }^{\circ}\text{C}$  in argon, the coating is completely crystalline and consists of phases of titanium oxide  $\text{TiO}$ , titanium nitride  $\text{Ti}_2\text{N}$  and titanium nickelide oxynitride  $\text{Ti}_4\text{Ni}_2\text{O}(\text{N})$ . The volume fraction of the  $\text{Ti}_2\text{N}$  phase does not exceed 7–10 vol.%. The major phases of the coating are  $\text{TiO}$  and  $\text{Ti}_4\text{Ni}_2\text{O}(\text{N,C})$ . The major component of the surface layers of the coating synthesized in nitrogen is the TiN phase. A group of low-intensity diffraction reflections from various phases,  $\text{TiO}_2(\text{N})$  (rutile),  $\text{Ti}_3\text{Ni}_4$ ,  $\text{Ti}_4\text{Ni}_2\text{N}(\text{O})$ ,  $\text{TiNiO}_3(\text{N})$ , with a total volume fraction of 15–20 vol.% was found. The TiNi(B2) and  $\text{TiNi}_3$  phases belong to the TiNi substrate and diffusion zone. All detected phases are completely crystalline.

Comparison of the data obtained by XRD, TEM and EDS methods made it possible to establish the belonging of each phase to the coating layers and build a phase formation scheme for coatings synthesized in an argon and a nitrogen atmosphere (Figure 6).

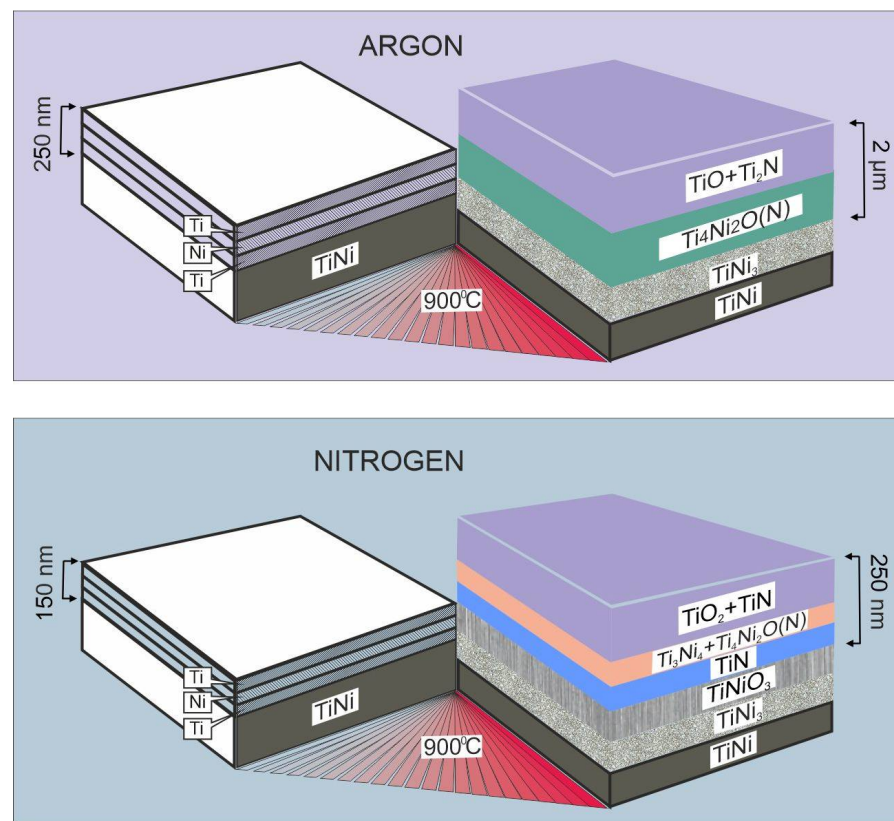


**Figure 6.** Scheme of the structure and phase composition of the coating obtained in argon and nitrogen atmospheres.

### 3.2.2. Study on Topographical Evolution and Wettability

Figure 7 shows the AFM images of the samples with a scan area of  $5\ \mu\text{m} \times 5\ \mu\text{m}$ . Topographic maps show that the surface of the TiNi substrate is smooth and has single irregularities, while the surfaces of the coatings synthesized in argon and nitrogen are rough. Small regular grains are observed on the surface of the coating synthesized in nitrogen. On the surface of the coating synthesized in argon, the grains are larger and coagulate, forming islands. The roughness results determined within the scanned area showed the following values:  $R_a = 11.93 \pm 5.71\ \text{nm}$  for a TiNi substrate;  $R_a = 33\ \text{nm}$  for synthesized coating in argon;  $R_a = 40.01 \pm 2.23\ \text{nm}$  for a coating synthesized in nitrogen. The increased cell adhesion in the form of a monolayer may be due to the uniform nanorough surface of the coating synthesized in nitrogen. There may also be a roughness threshold of up to  $1\ \mu\text{m}$ , above which cell proliferation becomes difficult [38].

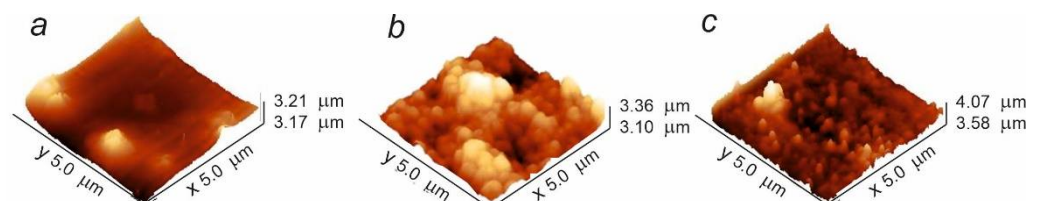


**Figure 7.** AFM topographical maps of uncoated TiNi substrate (a), coatings synthesized in argon (b) and nitrogen (c).

Surface topography affects cell adhesion and proliferation both in vitro and in vivo. Depending on the application, the implant must have a certain surface roughness: it can be smooth or more rough. Increasing the roughness on the nano/microscale gives the surface greater surface energy and wettability, which are some of the important properties that

affect cell–material interactions. The presence of uniform nanoroughness is favorable for the cell adhesion and proliferation and the formation of a monolayer of cells on the surface. Smoothness or low surface roughness reduce the ability of biological cells to adhere to the implant surface.

A comparative assessment of the surface electric potential distribution showed that the TiNi substrate is positively charged, in contrast to the synthesized coatings, where there are areas of negative and positive surface charge (Figure 8). This difference in polarization is caused by differences in surface topography and chemical composition. Structural studies showed that the upper layer of the coatings synthesized in argon and nitrogen are two-phase and consist of titanium nitrides and oxides of different modifications and with a different fraction. In this article, surface roughness and wetting properties have a greater influence on cell attachment and proliferation. The surface charge determines the amount, type and extent of absorbed proteins and thus the next process of cell adhesion. There are many studies on the effect of surface charge on cells. On the one hand, negative groups on the surface repel the cell at a great distance, but at a contact distance, they can firmly bind polarizable or amphoteric links of polymer chains in the cell membrane [39]. On the other hand, positively charged surfaces significantly affect cell adhesion and proliferation due to greater electrostatic attraction, especially in the early stages of cellular responses [40], since cells have a negative charge. However, there are also studies where cells multiply more actively on a negatively charged surface, and cell adhesion and proliferation on a positively charged biomaterial were suppressed [41]. Therefore, it is difficult to assess the effect of surface charge on cells.

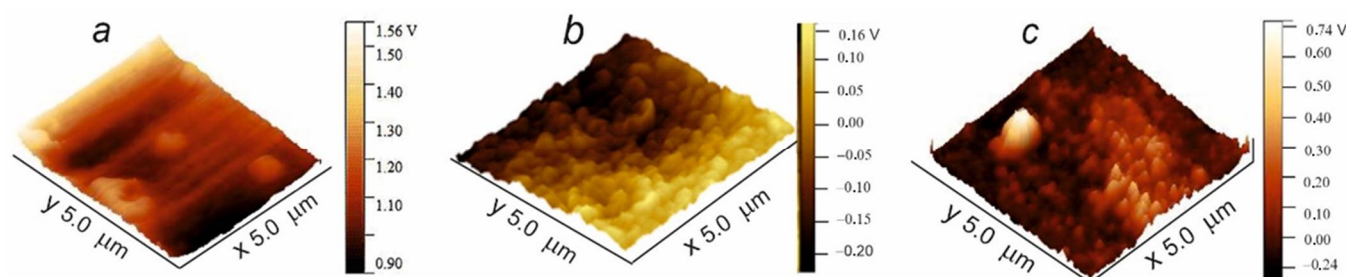


**Figure 8.** AFM surface potential map of uncoated TiNi substrate (a), coatings synthesized in argon (b) and nitrogen (c).

Wettability is an important property of implant surfaces that affects cell–material interactions. The sessile drop method was used to measure the contact wetting angle  $\theta$  of the surface of the substrate and synthesized coatings. Water was selected as the test liquid. The results of measuring the contact wetting angle showed that both synthesized coatings have a moderately hydrophilic surface. The contact angle of the coating synthesized in argon is  $53.1 \pm 0.44^\circ$ ; for the coating synthesized in nitrogen,  $\theta$  is  $59.6 \pm 0.42^\circ$  (Figure 9a). The surface of the TiNi substrate is hydrophobic and has  $\theta = 92.9 \pm 1.33$ . It is known that cell adhesion and proliferation are better manifested on a surface with moderate hydrophilicity, exhibiting a water contact angle  $\theta < 60^\circ$ , than on more hydrophobic or hydrophilic surfaces [35]. Hydrophobic surfaces show low attachment efficiency and long periods of induction before cells enter the exponential growth phase. On hydrophobic surfaces with poor cell–substrate compatibility, cells remain rounded for a long time compared to more compatible hydrophilic surfaces. However, if cells on poorly compatible surfaces survive, flattening occurs and, ultimately, a minor population of the surface. Our results on cytocompatibility show a correlation between the contact wetting angle and cell density, where we observe a high density of cell adhesion on hydrophilic surfaces. The cells cultured on the hydrophobic surface of the TiNi substrate did not form uniform cell layers, but rather separate locations.

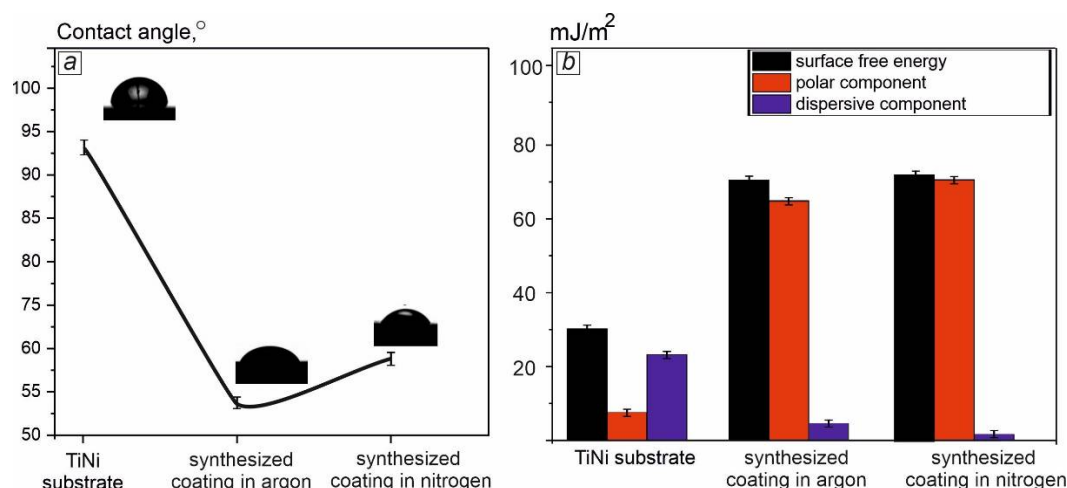


**Figure 9.** Contact angle (a) and surface free energy (b) values of the TiNi substrate, coating synthesized in argon atmosphere, coating synthesized in nitrogen atmosphere.

The surface free energy is  $30.25 \pm 0.74$  mJ/m<sup>2</sup> in TiNi substrate,  $70.17 \pm 0.44$  mJ/m<sup>2</sup> in the coating synthesized in argon and  $73.56 \pm 0.48$  mJ/m<sup>2</sup> in the coating synthesized in nitrogen (Figure 9b). It is known that an increase in surface energy occurs as a result of an increase in the surface area of grain boundaries [42], which correlates with scanning microscopic studies, where the outer layer of the coating synthesized in nitrogen has the smallest average grain size. Compared to the uncoated substrate, the synthesized coatings showed a significantly increased polar component and high total free surface energy. An increase in surface energy, in particular, an increase in the polar component of surface energy, has a positive effect on cell behavior and is responsible for adhesion and proliferation [43,44].

The biocompatible coating synthesized in a reactive nitrogen atmosphere is promising and, with further development of research, it can be used in medicine, for example, for long-term implants of ribs made of titanium and nickel–titanium alloys in thoracic surgery.

In the long term after implantation, when a strong biointerface is formed between the implant surface and the surrounding biological tissues, which transmits dynamic physiological loads, the adhesive strength of the protective coating is important for the biomechanical compatibility of implants. Thin, mechanically strong and electrochemically resistant coatings are able to successfully withstand complex cyclic deformation in a chemically aggressive organism environment without cracking and delamination. Therefore, the next stage of the research is the assessment of the stress–strain state of the coating under physiological loads using computational simulation [45,46].

#### 4. Conclusions

Reaction annealing of the deposited Ti/Ni/Ti nanolaminate at a temperature of 900 °C in an Ar atmosphere and a N<sub>2</sub> atmosphere led to the formation of a gradient crystalline coating. Reaction annealing in Ar leads to the formation of a dense two-layer coating 2.0–2.1 µm thick: layer I (TiO + Ti<sub>2</sub>N) + layer II (Ti<sub>4</sub>Ni<sub>2</sub>O(N)). Reaction annealing in N<sub>2</sub> leads to the formation of a thin three-layer nanocoating 250 nm thick: I (TiO<sub>2</sub> + TiN), II (Ti<sub>4</sub>Ni<sub>2</sub>N(O) + Ti<sub>3</sub>Ni<sub>4</sub>), III (TiN). No trace of nickel in the outer layers of the synthesized coatings was detected.

Coatings cause hemolysis of less than 1.5%, which corresponds to the acceptable hemolysis limit (ISO 10993–4:2018). At the same time, the uncoated polished TiNi substrate negatively affects blood erythrocytes and causes a degree of hemolysis of  $3.6\% \pm 0.8$ , higher than the permissible standard. The most cytotoxic sample is the intact TiNi substrate. The cytotoxicity of the coating synthesized in nitrogen is half that of the coating synthesized in argon.



The synthesized coatings are moderately hydrophilic, the contact angles of water wetting decreased relative to the values obtained on the uncoated substrate samples, from  $92.9 \pm 1.33$  to  $59.6 \pm 0.42^\circ$  for the coating synthesized in nitrogen and to  $53.1 \pm 0.44^\circ$  for coatings synthesized in argon. In this case, the surface energy of the synthesized coatings in Ar and N<sub>2</sub> reaches the values of  $67.17 \pm 0.44$  mJ/m<sup>2</sup> and  $73.56 \pm 0.48$  mJ/m<sup>2</sup>, respectively.

A cell adhesion study showed that  $90 \pm 5\%$  of the coating surface obtained with the nitrogen participation is covered with cell mass; on the coating obtained with the argon participation, the cells occupy  $70 \pm 5\%$ ; on the surface of the TiNi substrate, the cells cover less than 50%.

Thus, the moderately hydrophilic surface of the coating synthesized in nitrogen with a roughness parameter  $R_a = 40.01 \pm 2.23$  nm and high surface energy of  $73.56 \pm 0.48$  mJ/m<sup>2</sup> favorably influenced the cell adhesion and proliferation and the formation of a cell monolayer on the entire surface.

**Author Contributions:** Conceptualization, E.M., G.B. and Y.Y.; methodology, E.M., G.B. and O.K.; formal analysis, E.M. and O.K.; resources, E.M. and G.B.; writing—original draft preparation, G.B., E.M. and O.K.; writing—review and editing, E.M. and G.B.; supervision, E.M. and G.B.; project administration, G.B.; funding acquisition, G.B. and A.V. All authors have read and agreed to the published version of the manuscript.

**Funding:** This study was supported by the Tomsk State University Development Programme (Priority-2030).

**Institutional Review Board Statement:** The study was conducted in accordance with the Declaration of Helsinki and approved by Bioethical Committee of Tomsk State (approval protocol code number No 20/1116/2017).

**Data Availability Statement:** Not applicable.

**Acknowledgments:** The structure research was carried out with the equipment of Tomsk Regional Core Shared Research Facilities Center of National Research Tomsk State University (Grant of the Ministry of Science and Higher Education of the Russian Federation no. 075–15-2021–693 (no. 13.RFC.21.0012)).

**Conflicts of Interest:** The authors alone are responsible for the content and declare that there is no conflict of interests. The authors have no financial interest in the products presented in this report.

## References

1. Casaletto, M.P.; Ingo, G.M.; Kaciulis, S.; Mattogno, G.; Pandolfi, L.; Scavia, G. Surface studies of in vitro biocompatibility of titanium oxide coatings. *Appl. Surf. Sci.* **2001**, *172*, 167–177. [\[CrossRef\]](#)
2. Liu, M.; Li, J.; Zhang, Y. Recent advances in corrosion research of biomedical NiTi shape memory alloy. *Rare Met. Mater. Eng.* **2021**, *50*, 4165–4173.
3. Wang, J.; Wang, T.; Dong, S.; Kang, X.; Zhao, S.; Shi, H.; Gao, B.; Ma, S.; Liu, M.; Niu, L.; et al. The effect of Cu-doping on the corrosion behavior of NiTi alloy arch wires under simulated clinical conditions. *Mater. Res. Express* **2021**, *8*, 016537. [\[CrossRef\]](#)
4. Jin, S.; Zhang, Y.; Wang, Q.; Zhang, D.; Zhang, S. Influence of TiN coating on the biocompatibility of medical NiTi alloy. *Colloids Surf B Biointerfaces* **2013**, *101*, 343–349. [\[CrossRef\]](#)
5. Pisanec, S.; Ciacchi, L.C.; Vesselli, E.; Comelli, G.; Sbaizero, O.; Meriani, S.; De Vita, A. Bioactivity of TiN-coated titanium implants. *Acta Mater.* **2004**, *52*, 1237–1245. [\[CrossRef\]](#)
6. Zhao, L.F.; Hong, Y.; Yang, D.Y.; Lü, X.Y.; Xi, T.F.; Zhang, D.Y.; Hong, Y.; Yuan, J.F. The underlying biological mechanisms of biocompatibility differences between bare and TiN-coated NiTi alloys. *Biomed. Mater.* **2011**, *6*, 025012. [\[CrossRef\]](#)
7. Zuo, J.; Xie, Y.; Zhang, J.; Wei, Q.; Zhou, B.; Luo, J.; Wang, Y.; Yu, Z.M.; Tang, Z.G. TiN coated stainless steel bracket: Tribological, corrosion resistance, biocompatibility and mechanical performance. *Surf. Coat. Technol.* **2015**, *277*, 227–233. [\[CrossRef\]](#)
8. Nikolova, M.; Nikolova, V.; Ivanova, V.L.; Valkov, S.; Petrov, P.; Apostolova, M. Mechanical properties and in vitro biocompatibility evaluation of TiN/TiO<sub>2</sub> coated Ti6Al4V alloy. *Mater. Today Proc.* **2020**, *33*, 1781–1786. [\[CrossRef\]](#)
9. Luo, Q.; Yang, S.; Cooke, K.E. Hybrid HIPIMS and DC magnetron sputtering deposition of TiN coatings: Deposition rate, structure and tribological properties. *Surf. Coat. Technol.* **2013**, *236*, 13–21. [\[CrossRef\]](#)
10. Aissani, L.; Alhussein, A.; Ayad, A.; Nouveau, C.; Zgheib, E.; Belgroune, A.; Zaabat, M.; Barille, R. Relationship between structure, surface topography and tribo-mechanical behavior of Ti-N thin films elaborated at different N<sub>2</sub> flow rates. *Thin Solid Film.* **2021**, *724*, 138598. [\[CrossRef\]](#)



11. Kehal, A.; Saoula, N.; Nouveau, C. Effect of Ar/N<sub>2</sub> flow ratio on the microstructure and mechanical properties of Ti-Cr-N coatings deposited by DC magnetron sputtering on AISI D2 tool steels. *Surf. Coat. Technol.* **2021**, *421*, 127444. [\[CrossRef\]](#)
12. Oliveira, J.C.; Fernandes, F.; Serra, R.; Cavaleiro, A. On the role of the energetic species in TiN thin film growth by reactive deep oscillation magnetron sputtering in Ar/N. *Thin Solid Film.* **2017**, *645*, 253–264. [\[CrossRef\]](#)
13. Oghenevweta, J.E.; Wexler, D.; Calka, A. Understanding reaction sequences and mechanisms during synthesis of nanocrystalline Ti<sub>2</sub>N and TiN via magnetically controlled ball milling of Ti in nitrogen. *J. Mater. Sci.* **2017**, *53*, 3064–3077. [\[CrossRef\]](#)
14. Yue-Lin, L.; Shuo, J.; Ying, Z. Interaction between impurity nitrogen and tungsten: A first-principles investigation. *Chin. Phys. B* **2012**, *21*, 016105. [\[CrossRef\]](#)
15. Çahaa, I.; Alves, A.C.; Affonso, L.J.; Lisboa-Filho, P.N.; da Silva, J.H.D.; Rocha, L.A.; Pinto, A.M.P.; Toptan, F. Corrosion and tribocorrosion behaviour of titanium nitride thin films grown on titanium under different deposition times. *Surf. Coat. Technol.* **2019**, *374*, 878–888. [\[CrossRef\]](#)
16. Chaplanov, A.M.; Shcherbakova, E.N. Structural and phase transformations in thin titanium films under irradiation with nitrogen-hydrogen plasma. *Tech. Phys.* **1999**, *69*, 102–108. [\[CrossRef\]](#)
17. Datta, S.; Das, M.; Balla, V.K.; Bodhak, S.; Murugesan, V.K. Mechanical, wear, corrosion and biological properties of arc deposited titanium nitride coatings. *Surf. Coat. Technol.* **2018**, *344*, 214–222. [\[CrossRef\]](#)
18. Premnath, P.; Tavangar, A.; Tan, B.; Venkatakrishnan, K. Tuning cell adhesion by direct nanostructuring silicon into cell repulsive/adhesive patterns. *Exp. Cell Res.* **2015**, *337*, 44–52. [\[CrossRef\]](#)
19. Liao, S.-C.; Chen, C.-Y.; Hsu, Y.-H.; Li, C.-T.; Hsieh, C.-C.; Tsai, M.-S.; Chan, M.-Y.; Lee, C.-H.; Wang, S.-H.; Ng, S.-K.; et al. In vitro and in vivo biocompatibility study of surface modified TiN deposited on Ti6Al4V using high-power impulse magnetron sputtering technique. *Surf. Coat. Technol.* **2020**, *394*, 125814. [\[CrossRef\]](#)
20. Anusha Thampi, V.V.; Chukwuikea, V.I.; Shtansky, D.V.; Subramanian, B. Biocompatibility study of nanocomposite titanium boron nitride (TiBN) thin films for orthopedic implant applications. *Surf. Coat. Technol.* **2021**, *410*, 126968. [\[CrossRef\]](#)
21. Bai, J.; Gao, J.; Zhang, M.; Zheng, K.; Cao, Y.; Mao, Y.; Yu, S.; He, Z. Microwave plasma oxidation of near-equiatomic NiTi alloy for obtaining low-Ni TiO<sub>2</sub> coating. *Surf. Coat. Technol.* **2021**, *428*, 127883. [\[CrossRef\]](#)
22. Mahmud, A.; Wu, Z.; Zhang, J.; Liu, Y.; Yang, H. Surface oxidation of NiTi and its effects on thermal and mechanical properties. *Intermetallics* **2018**, *103*, 52–62. [\[CrossRef\]](#)
23. Wu, Z.; Mahmud, A.; Zhang, J.; Liu, Y.; Yang, H. Surface oxidation of NiTi during thermal exposure in flowing argon environment. *Mater. Des.* **2018**, *140*, 123–133. [\[CrossRef\]](#)
24. Yuan, B.; Li, H.; Gao, Y.; Chung, C.; Zhu, M. In vitro and in vivo evaluation of porous NiTi alloy modified by sputtering a surface TiO<sub>2</sub> film. *Sci. China Technol. Sci.* **2011**, *55*, 437–444. [\[CrossRef\]](#)
25. Wong, M.H.; Cheng, F.T.; Man, H.C. Laser oxidation of NiTi for improving corrosion resistance in Hanks' solution. *Mater. Lett.* **2007**, *61*, 3391–3394. [\[CrossRef\]](#)
26. Huang, C.-F.; Cheng, H.-C.; Liu, C.-M.; Chen, C.-C.; Ou, K.-L. Microstructure and phase transition of biocompatible titanium oxide film on titanium by plasma discharging. *J. Alloy. Compd.* **2009**, *476*, 683–688. [\[CrossRef\]](#)
27. Pana, I.; Braic, V.; Dinu, M.; Mouele, E.S.M.; Parau, A.C.; Petrik, L.F.; Braic, M. In Vitro Corrosion of Titanium Nitride and Oxynitride-Based Biocompatible Coatings Deposited on Stainless Steel. *Coatings* **2020**, *10*, 710. [\[CrossRef\]](#)
28. Hussein, M.A.; Madhan Kumar, A.; Anka, N.; Azeem, M.A. Thermal treatment effect on the surface and in vitro corrosion characteristics of arc deposited TiN coating on Ti alloy for orthopedic applications. *Ceram. Int.* **2021**, *47*, 23203–23213. [\[CrossRef\]](#)
29. Tsyganov, I.A.; Maitz, M.F.; Richter, E.; Reuther, H.; Mashina, A.I.; Rustichelli, F. Hemocompatibility of titanium-based coatings prepared by metal plasma immersion ion implantation and deposition. *Nucl. Instrum. Methods Phys. Res. B* **2007**, *257*, 122–127. [\[CrossRef\]](#)
30. Surovtseva, M.A. Titanium oxide- and oxynitride-coated nitinol: Effects of surface structure and composition on interactions with endothelial cells. *Appl. Surf. Sci.* **2022**, *578*, 152059. [\[CrossRef\]](#)
31. Karjalainen, P. Neointimal coverage and vasodilator response to titanium-nitrideoxide-coated bioactive stents and everolimus-eluting stents in patients with acute coronary syndrome: Insights from the BASE-ACS trial. *Int. J. Cardiovasc. Imaging* **2013**, *29*, 1693–1703. [\[CrossRef\]](#) [\[PubMed\]](#)
32. Marchenko, E.S.; Baigonakova, G.A.; Dubovikov, K.M.; Yasenchuk, Y.F.; Gunther, S.V. Reaction synthesis of gradient coatings by annealing of three-layer Ti–Ni–Ti nanolaminate magnetron sputtered on the TiNi substrate. *Surf. Interfaces* **2021**, *24*, 101111. [\[CrossRef\]](#)
33. Baigonakova, G.; Marchenko, E.; Yasenchuk, Y.; Kokorev, O.; Vorozhtsov, A.; Kulbakin, D. Microstructural characterization, wettability and cytocompatibility of gradient coatings synthesized by gas nitriding of three-layer Ti/Ni/Ti nanolaminates magnetron sputtered on the TiNi substrate. *Surf. Coat. Technol.* **2022**, *436*, 125543. [\[CrossRef\]](#)
34. Marchenko, E.; Yasenchuk, Y.; Baigonakova, G.; Gunther, S.; Yuzhakov, M.; Zenkin, S.; Potekae, A.; Dubovikov, K. Phase formation during air annealing of Ti–Ni–Ti laminate. *Surf. Coat. Technol.* **2020**, *388*, 125543. [\[CrossRef\]](#)
35. Liu, X.; Lim, J.Y.; Donahue, H.J.; Dhurjati, R.; Mastro, A.M.; Vogler, E.A. Influence of substratum surface chemistry/energy and topography on the human fetal osteoblastic cell line hFOB 1.19: Phenotypic and genotypic responses observed in vitro. *Biomaterials* **2007**, *28*, 4535–4550. [\[CrossRef\]](#)
36. Ding, X.; Xu, S.; Li, S.; Guo, Z.; Lu, H.; Lai, C.; Wu, J.; Wang, J.; Zeng, S.; Lin, X.; et al. Biological effects of titanium surface charge with a focus on protein adsorption. *ACS Omega* **2020**, *5*, 25617–25624. [\[CrossRef\]](#)

37. Movchan, B.A.; Demchishin, A.V. Structure and properties of thick condensates of nickel, titanium, tungsten, aluminum oxides, and zirconium dioxide in vacuum. *Phys. Met. Metallogr.* **1969**, *28*, 653.
38. Ponsonnet, L.; Reybier, K.; Jaffrezic, N.; Comte, V.; Lagneau, C.; Lissac, M.; Martelet, C. Relationship between surface properties (roughness, wettability) of titanium and titanium alloys and cell behavior. *Mater. Sci. Eng.* **2003**, *23*, 551–560. [[CrossRef](#)]
39. Maroudas, N.G. Adhesion and spreading of cells on charged surfaces. *J. Theor. Biot.* **1975**, *49*, 417–424. [[CrossRef](#)]
40. Metwally, S.; Stachewicz, U. Surface potential and charges impact on cell responses on biomaterials interfaces for medical applications. *Mater. Sci. Eng.* **2019**, *104*, 109883. [[CrossRef](#)]
41. Guo, C.Y.; Matinlinna, J.P.; Hong Tang, T.A. Effects of surface charges on dental implants: Past, present, and future. *Int. J. Biomater.* **2012**, *5*, 381535. [[CrossRef](#)] [[PubMed](#)]
42. Kieswetter, K.; Schwartz, Z.; Dean, D.D.; Boyan, B.D. The role of implant surface characteristics in the healing of bone. *Crit. Rev. Oral. Biol. Med.* **1996**, *7*, 329–345. [[CrossRef](#)] [[PubMed](#)]
43. Surmeneva, M.A.; Kleinhans, C.; Vacun, G.; Kluger, P.J.; Schddotonhaar, V.; Muller, M.; Hein, S.B.; Wittmar, A.; Ulbricht, M.; Prymak, O.; et al. Nano-hydroxyapatite-coated metal-ceramic composite of irontricalcium phosphate: Improving the surface wettability, adhesion and proliferation of mesenchymal stem cells in vitro. *Colloids Surf. B Biointerfaces* **2015**, *135*, 386–393. [[CrossRef](#)]
44. Redey, S.A.; Nardin, M.; Bernache-Assolant, D.; Rey, C.; Delannoy, P.; Sedel, L.; Marie, P.J. Behavior of human osteoblastic cells on stoichiometric hydroxyapatite and type A carbonate apatite: Role of surface energy. *J. Biomed. Mater. Res.* **2000**, *50*, 353–364. [[CrossRef](#)]
45. Ammarullah, M.I.; Santoso, G.; Sugiharto, S.; Supriyono, T.; Kurdi, O.; Tauviqirrahman, M.; Winarni, T.I.; Jamari, J. Tresca Stress Study of CoCrMo-on-CoCrMo Bearings Based on Body Mass Index Using 2D Computational Model. *J. Tribol.* **2022**, *33*, 31–38.
46. Chen, Y.; Guo, H.; Sun, M.; Lv, X. Tensile Mechanical Properties and Dynamic Constitutive Model of Polyurea Elastomer under Different Strain Rates. *Polymers* **2022**, *14*, 3579. [[CrossRef](#)]